Available online at www.sciencedirect.com
ScienceDirect
Journal of Power Sources 176 (2008) 46–53
JOURNAL OF POWER SOURCES
www.elsevier.com/locate/jpowsour

Preparation and characterization of coke resistant Ni/SiO_2 catalyst for carbon dioxide reforming of methane

Yun-Xiang Pan, Chang-Jun Liu *, Peng Shi

Key Laboratory for Green Chemical Technology of Ministry of Education, School of Chemical Engineering and Technology, Tianjin University, Tianjin 300072, PR China

Received 23 September 2007; received in revised form 12 October 2007; accepted 12 October 2007
Available online 22 October 2007

Abstract

Silica supported Ni catalyst is highly active for the CO_2 reforming of methane but it has poor stability due to coke formation. In this work, a glow discharge plasma was applied for the decomposition of nickel nitrate on the SiO_2 support, followed by thermal calcination in air. The plasma treatment enhances the interactions between the Ni particles and the silica and significantly improves the Ni dispersion. The plasma-treated Ni/SiO_2 catalyst exhibits comparable activity to the Ni/SiO_2 catalyst prepared by the thermal method without plasma treatment. The coke resistance of the Ni/SiO_2 catalyst is significantly enhanced by the plasma treatment.

Keywords: Ni/SiO_2; Plasma; Methane; CO_2 reforming; Coke resistance

1. Introduction

The CO_2 reforming of methane has great potential to provide a practical method for conversion of methane and carbon dioxide, the two major greenhouse gases [1]. This process generates synthesis gas ($CO + H_2$) with a H_2/CO ratio of 1:1 which is suitable for further synthesis reactions and fuel cell applications [2]. The CO_2 reforming of methane is also a promising method for the utilization of biogas and natural gas containing large amounts of CO_2 [3]. Fundamental issues of catalysis like structure-sensitive surfaces, carbon nanotubes as well as others have also made the CO_2 reforming be one of the frontiers in catalytic investigations.

Various catalysts, including Ni-based catalysts and supported noble metal catalysts, have been investigated for the CO_2 reforming of methane [3–7]. Ni-based catalysts exhibit high activity but a major problem is their deactivation due to coke formation [5]. Supported noble metal catalysts are less sensitive to coke formation. However, their limited availability and expensive prices make them less favored for practical applications [4,5]. Therefore the development of coke resistant Ni-based catalysts for CO_2 reforming is desirable [5,7].

Many efforts have been made to develop coke resistant nickel catalysts. A general approach is the selective blockage of some of the Ni particle defect sites using inert element atoms. Several elements have been used including S [8], Sn [9], Au [10] and alkali and alkaline earth metals, such as K and Ca [11,12]. These atoms are preferentially localized on the Ni particle defect sites. The methane dissociation rate is moderately decreased, and thus a better carbon formation–gasification balance is obtained, which leads to good coke resistance. However, this approach is usually accompanied by a decrease in the activity. Another approach is the addition of active noble metals, for example, Ru, Rh or Pt, to the Ni catalysts to improve the coke resistance ability [13–16]. In contrast to the passivation with sulfur or the addition of alkali or alkaline earth metals, addition of noble metals improves the activity. It has been suggested that the formation of alloys [13,14] or an improvement of the nickel dispersion [15,16] is responsible for the improvement of both the activity and the stability.

The metal–support interaction is one of the key influencing factors that affect the coke formation properties of the catalyst [7,17–19]. Weaker interactions between the metal and the support result in the catalyst being more susceptible to coking [7,17]. In order to enhance the metal–support interaction, several novel and interesting preparation methods or modification techniques have been exploited, especially for Ni-based catalysts [18,20–24]. For example, Che et al. [23] reported a

* Corresponding author. Tel.: +86 22 27406490; fax: +86 22 27890078.
E-mail address: ughg_cjl@yahoo.com (C.-J. Liu).

0378-7753/$ – see front matter © 2007 Elsevier B.V. All rights reserved.
doi:10.1016/j.jpowsour.2007.10.039

two-step method for the preparation of a Ni/SiO_2 catalyst with enhanced interactions between Ni and SiO_2. The first step was the formation of nickel nuclei that have strong interactions with the silica. Then the product of the first step was impregnated with nickel nitrate and nickel particle growth on the nuclei was achieved.

Recently, we developed a glow discharge plasma catalyst preparation technique to enhance the Ni–support interactions and to improve the dispersion, activity and coke resistance performance of Ni/Al_2O_3 catalysts for CO_2 reforming [21]. Glow discharge is a conventional non-thermal plasma, which is characterized by high electron temperatures (10,000–100,000 K) and low gas temperatures (as low as room temperature) [25,26]. The energetic species (electrons, ions and radicals) in plasma can modify the metal particle sizes, the metal morphology and the metal–support interactions of the catalyst [27]. Ni/SiO_2 catalyst has high activity for CO_2 reforming of methane but because of the weak interactions between Ni and SiO_2 the coke formation on this catalyst is more serious than for Ni/Al_2O_3 [17,19]. In this work, a coke resistant Ni/SiO_2 catalyst was developed using the argon glow discharge plasma preparation. The results show that the plasma treatment enhanced the interactions between Ni and SiO_2 and significantly improved the coke resistance of Ni/SiO_2 catalyst for the CO_2 reforming of methane.

2. Experimental

2.1. Catalyst preparation

The Ni/SiO_2 catalyst (with 10 wt% of NiO) was prepared by incipient wetness impregnation method. The silica was obtained commercially ($S = 300–350\ m^2\ g^{-1}$; Institute of Chemical Engineering, Tianjin, China). Prior to use, the silica was calcined at 500 °C for 3 h. It was then impregnated with an aqueous solution of nickel nitrate for about 12 h. The obtained sample was divided into two parts. One part was dried at 110 °C for another 12 h and then thermally calcined at 500 °C for 4 h. The other part was treated by plasma before further thermally calcination at 500 °C for 4 h. The plasma treatment apparatus is shown in Fig. 1. The sample (about 0.4 g) was loaded in a quartz boat and placed in the 'positive column' region of the glow discharge. When the pressure in the discharge tube was about 100 Pa, the glow discharge plasma was generated by applying 900 V to the electrode using a high voltage amplifier (Trek, 20/20B). The signal input for the high voltage amplifier was supplied by a function/arbitrary waveform generator (Hewlett Packard, 33120A) with a 100 Hz square wave. Ultra high pure grade argon (>99.999%) was used as the plasma-forming gas. The details of glow discharge plasma have been described previously [25]. The discharge was initiated at room temperature without external heating or cooling. According to the infrared temperature measurements (Icron 100PHT), the heating effect of the glow discharge could be ignored and the temperature of the catalyst powder was close to room temperature. During the plasma treatment, the nickel nitrate was decomposed under the influence of the glow discharge. Thermal calcination was then conducted without the use of the glow discharge plasma. Specific nickel oxide species were formed on the support with high dispersion. Nickel oxide formed in this manner exhibits unique morphology [27]. After calcination in air, both the samples were pressed, crushed and sieved through 40–60 mesh sieves before use. The samples with and without plasma treatment are denoted as P-Ni/SiO_2 and C-Ni/SiO_2, respectively.

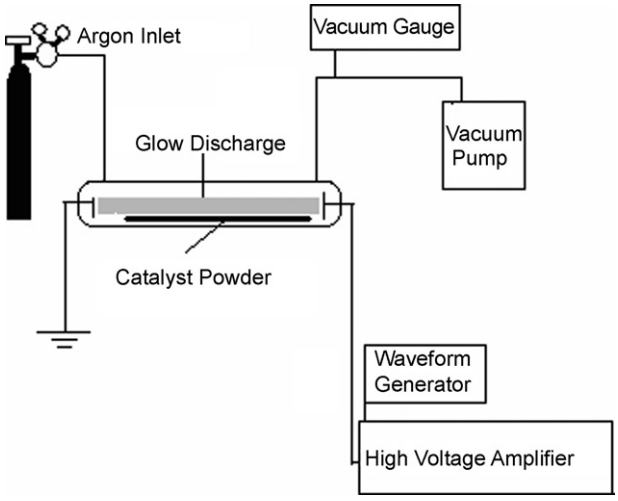

Fig. 1. Schematic for plasma modification apparatus.

2.2. Catalytic test

The CO_2 reforming of methane was conducted under atmospheric pressure in a quartz-tube fixed-bed reactor (i.d. 4 mm). Before the reaction, the catalyst (50 mg, 40–60 mesh) was reduced at 500 °C for 2 h in flowing hydrogen at a flow rate of 50 mL min^{-1}. Argon was used as dilution gas during the reaction. A gaseous mixture of methane, CO_2 and argon with a volume ratio of 1:1:2 was fed into the reactor at a space velocity of 48,000 mL (h gcat)$^{-1}$ (flow rate: 40 mL min^{-1}). The analysis of the effluent was carried out using an on-line gas chromatograph (Agilent 4890D) with a Porapak Q column and a thermal conductivity detector (TCD). A cold trap with ice was placed between the reactor exit and the GC sampling valve to remove the water formed during the reaction.

In this work, the conversions of methane and CO_2, the yields of hydrogen and CO and the H_2/CO ratio were calculated according to the following equations:

$$X(CH_4)\% = \frac{F_{CH_4,in} - F_{CH_4,out}}{F_{CH_4,in}} \times 100\%$$

$$X(CO_2)\% = \frac{F_{CO_2,in} - F_{CO_2,out}}{F_{CO_2,in}} \times 100\%$$

$$Y(H_2)\% = \frac{F_{H_2,out}}{2F_{CH_4,in}} \times 100\%$$

$$Y(CO)\% = \frac{F_{CO,out}}{F_{CO,out} + F_{CO_2,out} + F_{CH_4,out}} \times 100\%$$

$$R\left(\frac{H_2}{CO}\right) = \frac{Y(H_2)}{Y(CO)}$$

$$F_i = F_{total} C_i$$

where X, Y and F represent the conversion, yield and gas flow rate, respectively. F_{total} is the total flow rate of the feed gases or the gaseous effluent, and C_i is the molar fraction of component i in the feed gases or in the gaseous effluent.

2.3. Catalyst characterization

A hydrogen temperature programmed reduction experiment (H_2-TPR) was conducted in a fixed-bed reactor from 50 to 1000 °C, under 5% H_2/Ar (total flow rate: 30 mL min^{-1}) at atmospheric pressure. The reactor was the same as the one used for the catalytic activity test. The heating rate was set to 10 °C min^{-1}. The weight of the catalyst sample (40–60 mesh) was 100 mg. The H_2 ($m/z = 2$) and H_2O ($m/z = 18$) signals were continuously recorded by an on-line quadrupole mass spectrometer (GSD301, Ommistar^{TM}).

A temperature programmed oxidation (TPO) of the coke formed on the catalysts was also carried out in the reactor that was used for the catalytic activity test. The used catalyst sample (50 mg before reaction, 40–60 mesh) was heated in flowing 3% O_2/He at 30 mL min^{-1} over the temperature range 50–1000 °C at a heating rate of 10 °C min^{-1}. The CO ($m/z = 28$) and CO_2 ($m/z = 44$) signals were continuously recorded by the same mass spectrometer used for the H_2-TPR experiment.

CO chemisorption measurements of the catalyst were performed using a Quantachrome Autosorb-1-C system. These measurements determined the specific nickel surface area, the percent metal dispersion and the average crystallite size. The samples were degassed for 2 h at 300 °C before measurement and reduced at 500 °C in pure hydrogen at a flow rate of 30 mL min^{-1} for 2 h. The chemisorption measurements were conducted at 40 °C. Using an extrapolation method, the specific nickel surface area was calculated assuming a stoichiometric factor of 1 for the adsorption of CO on a nickel atom.

X-ray powder diffraction (XRD) patterns were recorded by an X′ Pert Pro diffractometer with a Co Kα radiation at a scanning rate of 4° min^{-1}. The phase identification was made by comparison to the Joint Committee on Powder Diffraction Standards (JCPDSs).

Transmission electron microscopy (TEM) observations of the fresh and used catalyst samples were performed using a Philips TECNAI G^{2}F20 system equipped with energy dispersion X-ray spectroscopy (EDX) operated at 200 kV. The samples were ground into fine powders and then ultrasonically dispersed in ethanol. A drop of the suspension was deposited on a carbon coated copper grid for the TEM analyses.

3. Results and discussion

3.1. H_2-TPR and XRD

The H_2-TPR profiles of the samples are shown in Fig. 2. For the C-Ni/SiO_2 sample, two reduction peaks at 330–500 and 500–620 °C are observed. However, for the P-Ni/SiO_2 sample, the first reduction peak is present at 320–500 °C, and the second one is between 500 and 680 °C. These H_2-TPR results are similar to those reported in the literature [22–24]. For both

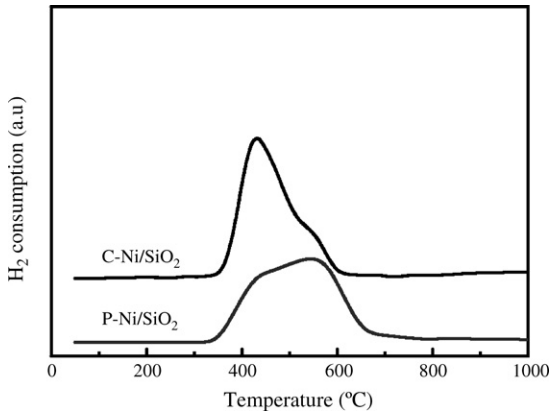

Fig. 2. H_2-TPR profiles of the C-Ni/SiO_2 and P-Ni/SiO_2 samples.

the samples, the lower temperature peak has been attributed to the reduction of the NiO that interacts weakly with the silica [3,23,24]. As the interaction between NiO and silica is enhanced, the reduction peak in the H_2-TPR profile shifts to a higher temperature [3,22]. Accordingly, the higher temperature peak for both the samples is assigned to the reduction of the NiO that strongly interacts with the silica. The second reduction peak in the P-Ni/SiO_2 sample is broader and more intense than in the C-Ni/SiO_2 sample. This indicates that the interactions between the Ni species and the silica are enhanced via the plasma treatment.

Fig. 3 shows the XRD patterns of different samples. A broad peak attributed to silica appears at about 25°. Peaks for the NiO crystal phase are observed in both the fresh C-NiO/SiO_2 and P-NiO/SiO_2 samples (Fig. 3b and c). After reduction at 500 °C for 2 h, peaks for Ni(1 1 1) and Ni(2 0 0) planes appear (Fig. 3d and e). The average size of Ni particles in the reduced C-Ni/SiO_2 and P-Ni/SiO_2 samples, estimated by Scherrer formula, is 10.2 and 7.6 nm, respectively. In both Fig. 3b and c, a very small peak is present at about 52°. According to the JCPDS files, only nickel silicate has an analogous XRD diffraction pattern at this position. This shows that some nickel silicate forms on both the fresh C-NiO/SiO_2 and P-NiO/SiO_2 samples. However, in the XRD patterns of the reduced samples, the nickel silicate peaks are covered by the big Ni peaks.

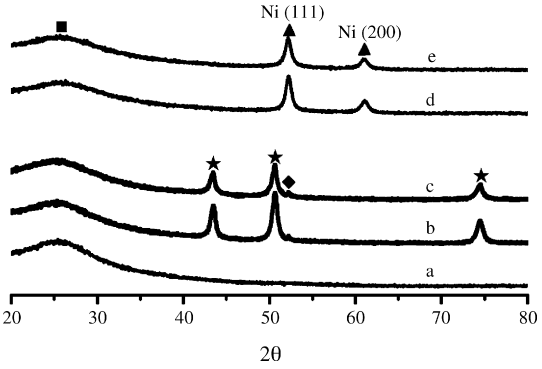

Fig. 3. XRD patterns of (a) SiO_2; (b) fresh C-NiO/SiO_2 sample; (c) fresh P-NiO/SiO_2 sample; (d) C-Ni/SiO_2 sample reduced at 500 °C for 2 h and (e) P-Ni/SiO_2 sample reduced at 500 °C for 2 h. ((■) SiO_2; (▲) Ni; (⋆) NiO; (♦) nickel silicate).

3.2. TEM and CO chemisorption

The TEM images of the reduced C-Ni/SiO_2 and P-Ni/SiO_2 samples are shown in Fig. 4. From Fig. 4a, it can be clearly seen that large Ni particles are present in the C-Ni/SiO_2 sample. Furthermore, aggregation of metal particles is clearly visible in C-Ni/SiO_2. In contrast, smaller Ni particles are homogeneously dispersed in the P-Ni/SiO_2 sample (Fig. 4b). The EDX result (Fig. 4c) confirms that these small particles appearing in the P-Ni/SiO_2 sample are all Ni^0. The smaller Ni particles and the homogeneous dispersion of these particles in the P-Ni/SiO_2 sample are ascribed to the enhanced interactions between the Ni particles and the silica. Fig. 5 shows the particle size distribution obtained from the TEM images of the C-Ni/SiO_2 and P-Ni/SiO_2 samples reduced at 500 °C for 2 h. In the C-Ni/SiO_2 sample, the particle sizes have a broad distribution, with the largest particle being 34.1 nm. On the other hand, the particle size distribution in the P-Ni/SiO_2 sample is much narrower and the sizes are between 3.4 and 10.1 nm. The number-weighted size of the Ni particles ($d_n = \sum n_i d_i / \sum n_i$; n_i: number of particles; d_i: size of particle i) is 13.1 and 5.4 nm for the C-Ni/SiO_2 and P-Ni/SiO_2 samples, respectively.

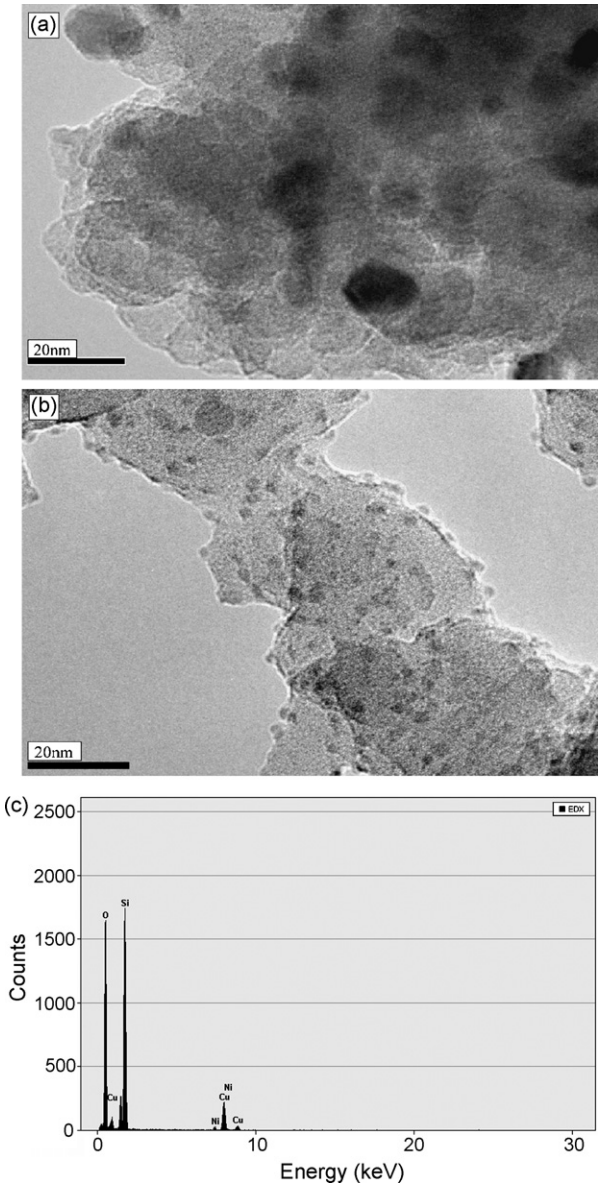

Fig. 4. TEM images of (a) C-Ni/SiO_2 and (b) P-Ni/SiO_2 samples after reduction at 500 °C for 2 h, and (c) EDX of the Ni particles observed in part (b).

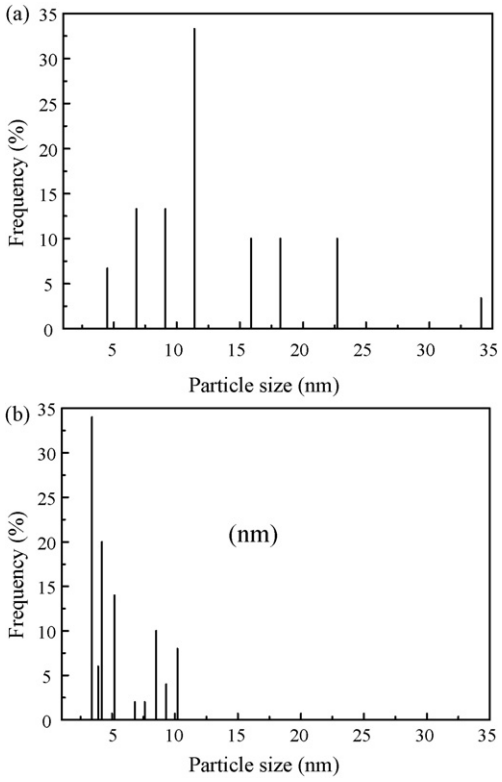

Fig. 5. Particle size distributions of (a) C-Ni/SiO_2 and (b) P-Ni/SiO_2 samples after reduction at 500 °C for 2 h.

High-resolution TEM images of the Ni particles in the reduced C-Ni/SiO_2 and P-Ni/SiO_2 samples are shown in Fig. 6. The crystallinity of the Ni particle in the P-Ni/SiO_2 sample is obviously higher than in the C-Ni/SiO_2 sample, showing that the plasma treatment can increase the crystallinity of the metal particles. Well-defined lattice fringes of the Ni(1 1 1) plane are observed in the P-Ni/SiO_2 sample (Fig. 6b). This indicates that uniformly crystallized particles with specific crystallographic plane are formed in the P-Ni/SiO_2 sample. The stronger metal–support interactions and the smaller Ni particles with higher dispersion lead to the formation of these uniformly crystallized particles. In the C-Ni/SiO_2 sample, the Ni particle surface appears to be a complicated combination of many crystallographic planes (Fig. 6a). This combination leads to high concentrations of distortions and lattice defects [28]. The low crystallinity of the Ni particles in the C-Ni/SiO_2 sample is ascribed to the migration and aggregation of the particles.

The Ni particles in the C-Ni/SiO_2 sample appear to have spherical shapes, but in the P-Ni/SiO_2 sample the Ni particles appear to be flattened and spread out on the support. Therefore, for the P-Ni/SiO_2 sample there are a larger contact interface and a smaller contact angle between the Ni particle and the support.

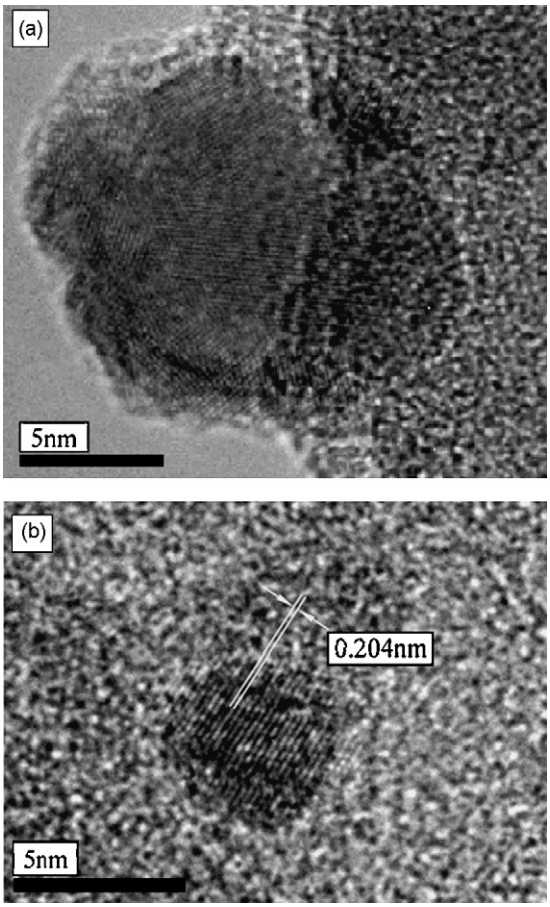

Fig. 6. High-resolution TEM images of the Ni particles in the (a) C-Ni/SiO_2 and (b) P-Ni/SiO_2 samples after reduction at 500 °C for 2 h.

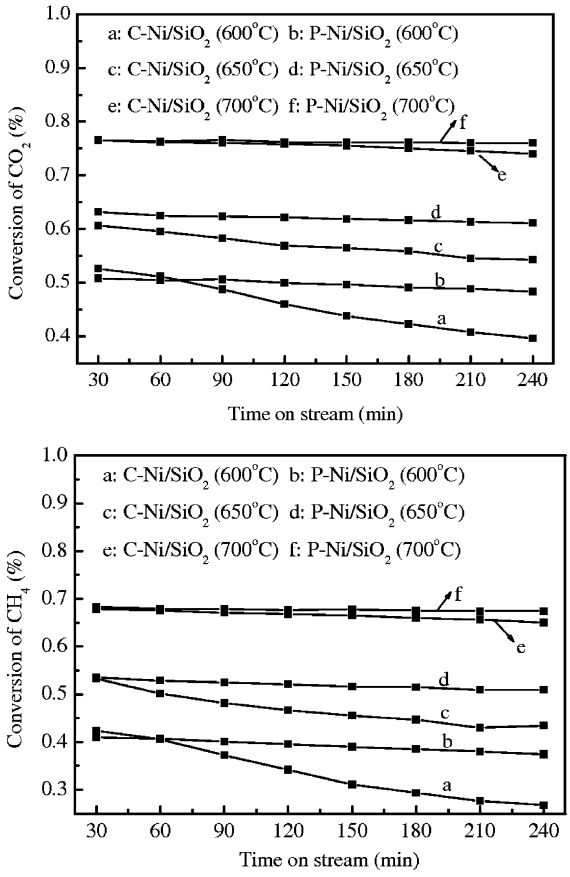

Fig. 7. Changes of conversions of carbon dioxide and methane over 4 h of reaction for the C-Ni/SiO_2 and P-Ni/SiO_2 samples at 600, 650 and 700 °C.

These effects produce strong interactions between the Ni particle and the support.

The CO chemisorption results are shown in Table 1. A higher dispersion of Ni is present in the P-Ni/SiO_2 sample. The average crystallite size of Ni particle in the P-Ni/SiO_2 sample is less than that in the C-Ni/SiO_2 sample. The average crystallite sizes of Ni particle obtained by CO chemisorpion are in good agreement with those calculated from the XRD and TEM results.

3.3. Catalytic test

Fig. 7 shows the activities of the C-Ni/SiO_2 and P-Ni/SiO_2 samples at 600, 650 and 700 °C. The conversion of carbon dioxide is slightly higher than that of methane, indicating that the reverse water gas shift reaction occurs [21,22]. The activity of the P-Ni/SiO_2 sample is comparable to the C-Ni/SiO_2 sample. However, significant deactivation is observed for the C-Ni/SiO_2 sample, especially at 600 and 650 °C. P-Ni/SiO_2 sample shows improved stability and changes of the conversions of carbon dioxide and methane over this sample are very slight. Coke formation could be the main reason for the deactivation of the C-Ni/SiO_2 sample. The changes of the synthesis gas ratio (H_2/CO) for C-Ni/SiO_2 and P-Ni/SiO_2 samples at different temperatures are shown in Table 2. For both of the samples and at all conditions, the ratios are smaller than 1. This is caused by the consumption of hydrogen by the reverse water gas shift reaction that occurs under our experimental conditions.

3.4. Coke formation

Figs. 8 and 9 show the TEM images of the C-Ni/SiO_2 and P-Ni/SiO_2 samples after the reaction at 700 °C for 4 h. In the TEM images of the used C-Ni/SiO_2 sample, a large amount of

Table 1
CO chemisorption results of the C-Ni/SiO_2 and P-Ni/SiO_2 samples after reduction at 500 °C for 2 h

Samples	Active metal surface area ($m^2\ g^{-1}$)	Metal dispersion (%)	Average crystallite size (nm)
C-Ni/SiO_2	5.7	10.7	9.4
P-Ni/SiO_2	9.1	17.0	5.9

Table 2
Changes of the H_2/CO ratio for the C-Ni/SiO_2 and P-Ni/SiO_2 samples at different temperatures

Samples	600 °C		650 °C		700 °C	
	0.5 h	4 h	0.5 h	4 h	0.5 h	4 h
C-Ni/SiO_2	0.85	0.68	0.87	0.76	0.99	0.98
P-Ni/SiO_2	0.87	0.82	0.89	0.83	0.97	0.96

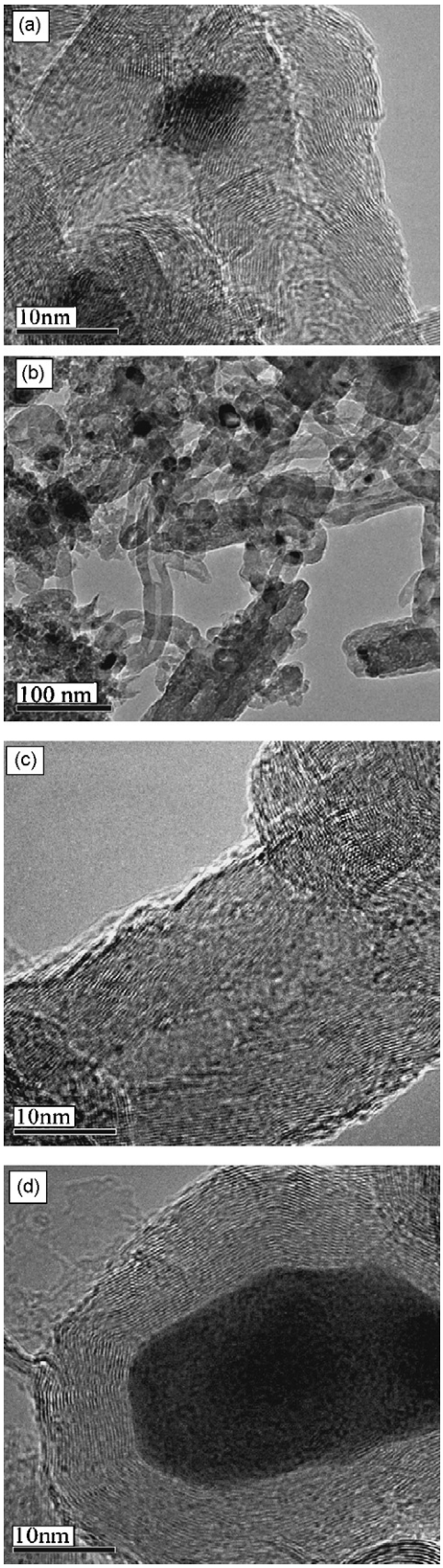

Fig. 8. TEM images of the C-Ni/SiO_2 sample after reaction at 700 °C for 4 h.

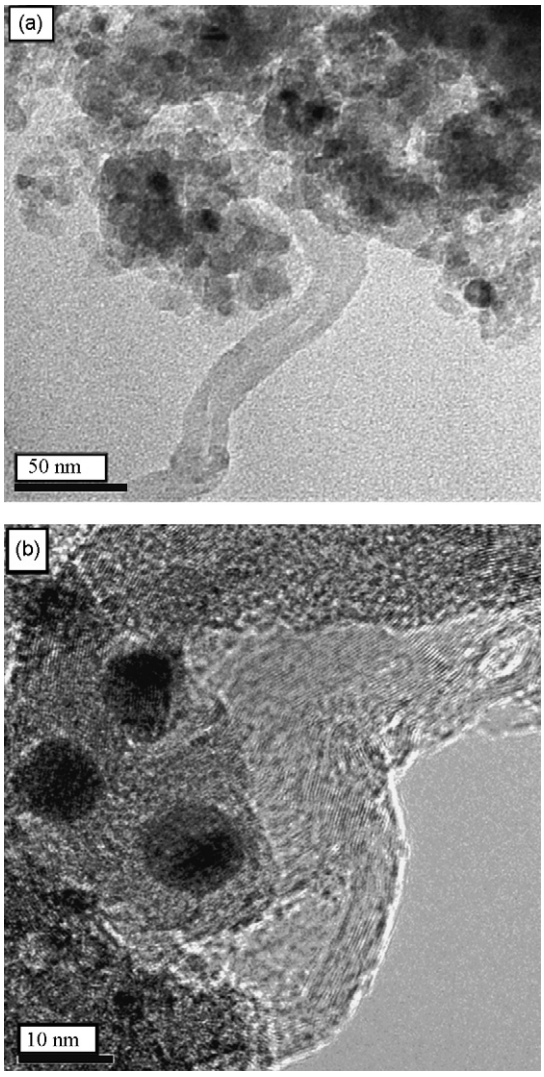

Fig. 9. TEM images of the P-Ni/SiO_2 sample after reaction at 700 °C for 4 h.

graphitic carbon and filamentous carbon can be observed. Some Ni particles are incorporated into the carbon species (Fig. 8a), which can lead to the formation of nickel carbide. In addition, some Ni particles are encapsulated in the graphite sheets, as shown in Fig. 8d. On the other hand, little filamentous carbon and graphitic carbon are observed in the TEM images of the used P-Ni/SiO_2 sample, even with careful examination. The TEM analyses confirm that the plasma-treated catalyst exhibits improved Ni dispersion and excellent resistance to the formation of filamentous carbon and encapsulating carbon. The TEM analyses also confirm that different carbon species are formed over the C-Ni/SiO_2 and P-Ni/SiO_2 samples. Further confirmation of this will be presented below with the TPO results.

The results of the TPO experiments on the used P-Ni/SiO_2 and C-Ni/SiO_2 samples are shown in Fig. 10. For the used C-Ni/SiO_2 sample, there are two peaks located at 518 and 732 °C, whereas for the used P-Ni/SiO_2 sample the peaks appear at 521 and 707 °C. During the TPO experiment, no carbon monoxide formation was observed. It has been suggested that Ni-based catalysts are active for the oxidation of carbon species, and the

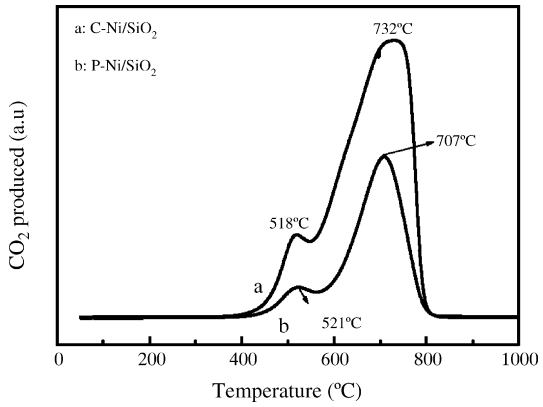

Fig. 10. TPO profiles of the C-Ni/SiO_2 and P-Ni/SiO_2 samples after reaction at 700 °C for 4 h.

distance between the carbon and the Ni particles can affect the oxidation temperature of the carbon species [29]. For example, because the oxygen molecules or atoms cannot attach to the Ni particles, the oxidation temperature of the carbon encapsulated Ni particles would be very high. Without a catalyst, the oxidation temperature of graphitic carbon is about 725 °C [29]. For the used C-Ni/SiO_2 sample, the peak at 732 °C may be caused by the oxidation of graphitic carbon covering or encapsulating the Ni particles. The peak at 518 °C is probably generated from the oxidation of nickel carbide, filamentous carbon or/and amorphous carbon. For the used P-Ni/SiO_2 sample, the peak at 707 °C is ascribed to the oxidation of the graphitic carbon, which is far away from the Ni particles or on the support. The peak at 521 °C for this sample may represent the oxidation of: (i) carbon adjacent to the Ni particles; (ii) filamentous carbon and/or (iii) amorphous carbon. The TPO profiles show that the amount of carbon deposited in the used P-Ni/SiO_2 sample is much less than that in the used C-Ni/SiO_2 sample, indicating an enhanced resistance of the P-Ni/SiO_2 sample to coking. The main reasons for the enhancement in the coke resistance are the stronger metal–support interactions and the smaller Ni particles with higher dispersion.

Methane decomposition over the surface of the Ni particles is the main source of the active carbon atoms. The carbon atoms can be gasified by carbon dioxide, which is the primary way to eliminate the carbon. The carbon formation–gasification balance is closely related to the rate of methane decomposition. If the gasification of the carbon atoms proceeds more slowly than the formation of the carbon atoms, these carbon atoms will precipitate and polymerize. Methane decomposition is structure sensitive. Particles with close packed planes (such as Ni(1 1 1)) have higher activation energy than those with distortions and lattice defects [30–32]. Due to the low crystallinity of the Ni particles in the C-Ni/SiO_2 sample, the precipitation of the carbon atoms readily proceeds in all directions around the particle [28]. Moreover, due to the weak interactions between the Ni particle and the silica, the carbon atoms can also easily enter into the interface between the Ni particle and the support. The precipitated carbon atoms gradually polymerize into carbon clusters [33] or carbon islands [34]. At low temperature, there is not enough energy to destroy the interactions between the islands and the Ni particles, so these islands continually increase in size on the surface of the particle until the particle is completely encapsulated [34]. Evidently, in the C-Ni/SiO_2 sample, the Ni particle is more easily encapsulated by the precipitated carbon.

In addition, the precipitated carbon atoms can diffuse through the Ni particle or along a given crystallographic plane. The diffusion of the carbon atoms through the Ni particles leads to the formation of filamentous carbon [35]. The high surface defect concentration of the Ni particle in the C-Ni/SiO_2 sample is more favorable for the diffusion of the carbon through the particles. Thus it is not surprising to observe so much filamentous carbon in the C-Ni/SiO_2 sample (Fig. 8b). It has been suggested that, usually, there are graphitic carbon caps or graphite steps at the interface between the filamentous carbon and the Ni particles [33,34]. The caps or steps can be clearly identified in Fig. 8c. The diffusion of the carbon atoms through the Ni particles can also cause the incorporation of Ni metal into the carbon species. This is seen in Fig. 8a. The diffusion of the carbon along a given crystallographic plane (e.g., the close packed Ni(1 1 1) plane) and the spillover of the carbon onto the surface of the support are the main source for the growth of the graphite layer.

4. Conclusion

A glow discharge plasma treatment technique has been used to prepare Ni/SiO_2 catalyst for the CO_2 reforming of methane. H_2-TPR and XRD results indicate that the plasma treatment enhances the interactions between the Ni particles and the silica. CO chemisorption and TEM characterization confirm that the size of Ni particles is smaller and the dispersion of the particles is more homogeneous in the plasma-treated Ni/SiO_2 catalyst. In addition, uniformly crystallized Ni particles with specific crystallographic plane are observed in the plasma-treated Ni/SiO_2 catalyst. The plasma-treated Ni/SiO_2 catalyst has comparable activity to the Ni/SiO_2 catalyst prepared by wetness impregnation method without plasma treatment. TPO and TEM results demonstrate that the plasma-treated Ni/SiO_2 catalyst shows enhanced resistance to coking. This enhancement is attributed to the stronger metal–support interactions and the smaller Ni particles with higher dispersion.

Acknowledgements

The support from the National Natural Science Foundation of China (under contract 20490203) and 973 project (under contract 2005CB221406) are greatly appreciated. The instruments supplied by ABB Switzerland are also appreciated.

References

[1] A. Kaengsilalai, A. Luengnaruemitchai, S. Jitkarnka, S. Wongkasemjit, J. Power Sources 165 (2007) 347–352.
[2] N. Laosiripojana, S. Assabumrungrat, J. Power Sources 163 (2007) 943–951.
[3] F. Pompeo, N.N. Nichio, M.G. González, M. Montes, Catal. Today 107–108 (2005) 856–862.
[4] J.R.H. Ross, Catal. Today 100 (2005) 151–158.
[5] M.C.J. Bradford, M.A. Vannice, Appl. Catal. A: Gen. 142 (1996) 73–96.

[6] S.B. Wang, G.Q.M. Lu, Energy Fuels 10 (1996) 896–904.
[7] S.B. Wang, G.Q.M. Lu, Appl. Catal. B: Environ. 16 (1998) 269–277.
[8] J.R. Rostrup-Nielsen, J.-H.B. Hansen, J. Catal. 144 (1993) 38–49.
[9] E. Nikolla, A. Holewinski, J. Schwank, S. Linic, J. Am. Chem. Soc. 128 (2006) 11354–11355.
[10] F. Besenbacher, I. Chorkendorff, B.S. Clausen, B. Hammer, A.M. Moelenbroek, J.K. Nørskov, I. Steensgaard, Science 279 (1998) 1913–1915.
[11] T. Osaki, T. Mori, J. Catal. 204 (2001) 89–97.
[12] J. Juan-Juan, M.C. Román-Martínez, M.J. Illán-Gómez, Appl. Catal. A: Gen. 301 (2006) 9–15.
[13] C. Crisafulli, S. Scirè, R. Maggiore, S. Minicò, S. Galvagno, Catal. Lett. 59 (1999) 21–26.
[14] C. Crisafulli, S. Scirè, S. Minicò, L. Solarino, Appl. Catal. A: Gen. 225 (2002) 1–9.
[15] Z.Y. Hou, T. Yashima, Catal. Lett. 89 (2003) 193–197.
[16] J.A.C. Dias, J.M. Assaf, J. Power Sources 130 (2004) 106–110.
[17] Z. Xu, Y.M. Li, J.Y. Zhang, L. Chang, R.Q. Zhou, Z.T. Duan, Appl. Catal. A: Gen. 210 (2001) 45–53.
[18] J.C. Yang, Y.G. Shul, C. Louis, M. Che, Catal. Today 44 (1998) 315–325.
[19] S.B. Wang, G.Q.M. Lu, Energy Fuels 12 (1998) 248–256.
[20] J.-G. Wang, C.-J. Liu, Y.-P. Zhang, K.-L. Yu, X.-L. Zhu, F. He, Catal. Today 89 (2004) 183–191.
[21] D.-G. Cheng, X.-L. Zhu, Y.-H. Ben, F. He, L. Cui, C.-J. Liu, Catal. Today 115 (2006) 205–210.
[22] S. Tomiyama, R. Takahashi, S. Sato, T. Sodesawa, S. Yoshida, Appl. Catal. A: Gen. 241 (2003) 349–361.
[23] M. Che, Z.X. Cheng, C. Louis, J. Am. Chem. Soc. 117 (1995) 2008–2018.
[24] C. Louis, Z.X. Cheng, M. Che, J. Phys. Chem. 97 (1993) 5703–5712.
[25] C.-J. Liu, G.P. Vissokov, B.W.-L. Jang, Catal. Today 72 (2002) 173–184.
[26] Z.-J. Wang, Y. Zhao, L. Cui, H. Du, P. Yao, C.-J. Liu, Green Chem. 9 (2007) 554–559.
[27] J.-J. Zou, C.-J. Liu, Y.-P. Zhang, Langmuir 22 (2006) 2334–2339.
[28] V.C.H. Kroll, H.M. Swaan, C. Mirodatos, J. Catal. 161 (1996) 409–422.
[29] P. Wang, E. Tanabe, K. Ito, J. Jia, H. Morioka, T. Shishido, K. Takehira, Appl. Catal. A: Gen. 231 (2002) 35–44.
[30] T.V. Choudhary, D.W. Goodman, J. Mol. Catal. A: Chem. 163 (2000) 9–18.
[31] H. Burghgraef, A.P.J. Jansen, R.A.V. Santen, Surf. Sci. 324 (1995) 345–356.
[32] J.R. Rostrup-Nielsen, J.K. Nørskov, Top. Catal. 40 (2006) 45–48.
[33] H.S. Bengaard, J.K. Nørskov, J. Sehested, B.S. Clausen, L.P. Nielsen, A.M. Molenbroek, J.R. Rostrup-Nielsen, J. Catal. 209 (2002) 365–384.
[34] F. Ding, A. Rosén, E.E.B. Campbell, L.K.L. Falk, K. Bolton, J. Phys. Chem. B 110 (2006) 7666–7670.
[35] S. Takenaka, S. Kobayashi, H. Ogihara, K. Otsuka, J. Catal. 217 (2003) 79–87.